

Quantum Optics and Laser 2021/22

REPORT 3 - BEAM OPTICS

Prof. Paolo Villoresi

Samuele Piccinelli

(Dated: 6 December, 2021)

Although the wave nature of light seems to preclude the possibility for it to be confined and transported in free space without angular spread, confined transport is indeed a reality in the form of beams that come as close as possible to spatially localised and non-diverging waves. This work is divided into three parts: in the first one we study the geometrical parameters that characterise the profile of a light beam under different experimental configurations; in the second one we will comment on some results for orbital angular momentum (OAM) waves. Finally, we will see an example of Fresnel diffraction - a phenomenon arising when an electromagnetic wave passing through an aperture is hitting a screen - and compute the characteristic size (e.g. radius) of the aperture. In the end, conclusions will be drawn.

1 GAUSSIAN BEAM DIVERGENCE

1.1 THEORETICAL BACKGROUND

A Gaussian beam is a beam of electromagnetic radiation with high monochromaticity whose amplitude envelope in the transverse plane is given by a Gaussian function, which in turn implies a Gaussian intensity profile. The importance of the transverse Gaussian mode is that it describes the intended output of most (but not all) lasers, as such a beam can be focused into the most concentrated spot.

The Gaussian beam is a transverse electromagnetic (TEM) mode, whose mathematical expression for the electric field amplitude is a solution to the **paraxial Helmholtz equation**. Assuming polarization in the x direction and propagation in the $+\hat{z}$ direction, the electric field is given by:

$$\mathbf{E}(\mathbf{r}, z) = E_0 \hat{\mathbf{x}} \frac{w_0}{w(z)} \exp\left(\frac{-\rho^2}{w(z)^2}\right) \exp\left(-i\left(kz + k\frac{r^2}{2R(z)} - \psi(z)\right)\right), \quad (1)$$

where

- ρ is the **radial distance** from the center axis of the beam;
- z is the **axial distance** from the beam's focus ("waist");
- $k = 2\pi n/\lambda$ is the **wave number** (in rad/m) for a free-space wavelength λ , and n is the index of refraction of the medium in which the beam propagates;
- $E_0 = E(0, 0)$ is the **electric field amplitude** (and phase) at the origin ($r = 0, z = 0$);
- $w(z)$ is the radius at which the intensity value decreases by a factor $1/e^2 \approx 0.135$ of their value on the beam axis: since 86% of the power is carried within a circle of radius $\rho = w(z)$, we regard $w(z)$ as the **beam width**;
- $w_0 = w(0)$ is the **waist radius**;
- $R(z)$ is the **radius of curvature** of the beam's wavefronts at z ;

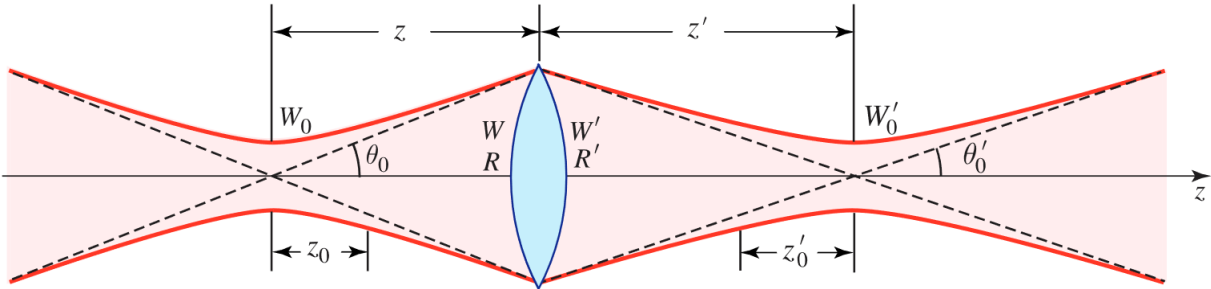


Figure 1: Transmission of a gaussian beam through a thin lens, as shown in [1].

- $\psi(z)$ is the **Gouy phase** at z , an extra phase term beyond that attributable to the phase velocity of light.

For a given wavelength and polarisation, the electric and magnetic field amplitude profiles along any circular Gaussian beam are determined by the **waist** (focus) w_0 (i.e. the minimum thickness of the beam). At any position z relative to the waist along a beam having a specified w_0 , the field amplitudes and phases are thereby determined. Likewise, the beam width profile $w(z)$ is completely determined by w_0 : the dependence of the beam width on z is governed by the hyperbolic relation

$$w(z) = w_0 \sqrt{1 + \left(\frac{z}{z_0}\right)^2}. \quad (2)$$

The beam width increases monotonically with z and $w(z = \pm z_0) = \sqrt{2}w_0$ (z_0 is known as the **Reyleigh range**); moreover, the beam radius $w(z)$, at any position z along the beam, is related to the full width at half maximum (FWHM) of the intensity distribution at that position according to

$$w(z) = \frac{\text{FWHM}}{\sqrt{2 \ln 2}} \equiv 2 \cdot \sigma \equiv 2 \cdot \text{RMS} \quad (3)$$

where σ is the width parameter for the intensity distribution.

When a gaussian beam is refocused by a lens, the transverse phase dependence is altered; this results in a different Gaussian beam (see Fig. 1). If we indicate with an apex the quantities of interest after the lens, for the waist radius it holds

$$w'_0 = M w_0 \quad (4)$$

$$(z' - f) = M^2(z - f), \quad (5)$$

where M is the **magnification factor** and f is the **focal length** of the lens.

1.2 EXPERIMENTAL SETUP

The experimental setup is composed of:

- A He-Ne laser ($\lambda = 633 \text{ nm}$) and related optical instrumentation (e.g.: filters, attenuators, etc.);
- A digital camera (resolution of 1280×1024 pixels), suitably interfaced with a computer to display the acquired image in real time, using a dedicated software;

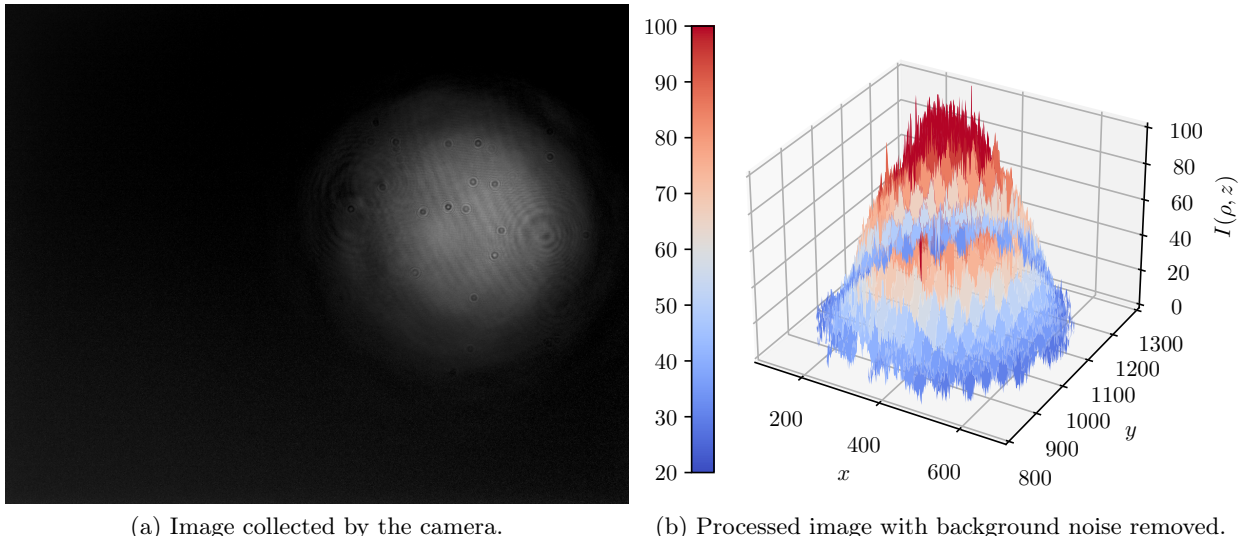


Figure 2: Example of the processing of raw images in the case with lens, $z = 50$ mm.

- In the second part of the experiment, a converging lens, designed to reshape the geometry of the beam generated by the source (see Fig. 1).

1.3 DATASET

The dataset consists of 22 and 16 images taken at different distances along a graduated ruler for the case with and without lens respectively. The approach described in the following section is based on the processing of these digital images of the beam spot acquired by the camera at varying distances from the lens.

Images are loaded and converted to a matrix of values representing the degree of brightness of the pixel. When present, background noise is subtracted from all input values. The positions along the ruler are considered without uncertainty in the following analysis; we consider the distance

- $d = 9$ cm, start of the ruler to laser source;
- $d_1 = 53.5$ cm, laser to lens;
- $d_2 = 2.7$ cm, lens to ruler.

Moreover, we take into account that the camera sensor is not exactly placed above the point used to take measurements on the ruler. Specifically, we further add an offset of around $d_{\text{off}} = 3.5$ cm in order to correctly define the position of the sensor.

An example of the processing of raw images is given in Fig. 2 for a distance of $z = 50$ mm.

1.4 ANALYSIS AND DISCUSSION

We consider the sections of the obtained three-dimensional model with a transverse plane (with respect to the beam axis) along an arbitrary direction and intersecting the peak of the graph: in this way it is possible to highlight the intensity profile of the beam. The diametrical extension of

z	$\sigma \pm \sigma_\sigma$ [μm]	z	$\sigma \pm \sigma_\sigma$ [μm]	z	$\sigma \pm \sigma_\sigma$ [μm]	z	$\sigma \pm \sigma_\sigma$ [μm]
0 mm	327 ± 1	110 mm	357 ± 1	50 mm	1316 ± 4	86.5 mm	33.29 ± 0.09
10 mm	333 ± 1	120 mm	360 ± 1	55 mm	1166 ± 5	90 mm	95.5 ± 0.2
20 mm	335 ± 1	130 mm	364 ± 1	60 mm	981 ± 4	95 mm	284.3 ± 0.9
30 mm	334 ± 2	150 mm	367 ± 2	65 mm	794 ± 3	100 mm	438 ± 2
40 mm	334 ± 2	200 mm	379 ± 1	70 mm	585 ± 4	105 mm	603 ± 1
50 mm	341 ± 1	250 mm	388 ± 1	75 mm	394 ± 1	110 mm	798 ± 2
60 mm	345 ± 2	300 mm	397 ± 2	80 mm	254.4 ± 0.7	115 mm	939 ± 3
70 mm	345 ± 1	350 mm	407 ± 1	85 mm	85.1 ± 0.3	120 mm	1118 ± 4
80 mm	350 ± 1	400 mm	418 ± 2				
90 mm	352 ± 1	450 mm	430 ± 1				
100 mm	355 ± 2	500 mm	444 ± 1				

Table 1: Setup with no lens.

$\langle \sigma \rangle$ obtained from the interpolation of the intensity distributions for each image.

the spot is assumed perfectly circular. Using the relation factor $\frac{\text{pixel size}}{\mu\text{m}}$ we convert the pixel values to distances.

We interpolate these curves with a gaussian function: for each image we save the values of the found σ along with its uncertainty. The final estimate is given by the mean of each of this sub-samples with the relative error of the mean. We report in Table 1, Table 2 the values obtained for the case without and with lens respectively. Note how the error in Table 2 gets smaller and smaller as we get closer to the Rayleigh range: this is due to the data analysis that select transverse planes containing a maximum of the intensity: when the beam is more focused the pixel saturate, the number of eligible planes increases and the error on the mean decreases consequently.

We interpolate with Eq. (2) the estimates of $\langle \sigma \rangle$ obtained, to get a final the values for w_0 , z_0 (Fig. 3) and w'_0 , z'_0 (Fig. 4) for the first and second setup respectively. In the second case the plot has been translated to the origin to aid fit convergence. The results, along with their uncertainties, are reported below.

$$\begin{aligned} w_0 &= (333 \pm 2) \text{ μm} & z_0 &= (685 \pm 19) \text{ mm} \\ w'_0 &= (35 \pm 34) \text{ μm} & z'_0 &= (684 \pm 1) \text{ mm}. \end{aligned}$$

Notice how the relative error increases for w_0 and decreases for z_0 : the points for the case with no lens concentrate along the right arm of the curve and thus leave more uncertainty in the determination of the vertex hyperbola, while for the case with lens the opposite holds.

By inverting Eq. (5) we can get an estimate of the focal length of the lens used; the relation $f = (zM^2 - z')/(M^2 - 1)$ yields to

$$f = (15.4 \pm 0.8) \text{ cm},$$

where the uncertainty is obtained through error propagation.

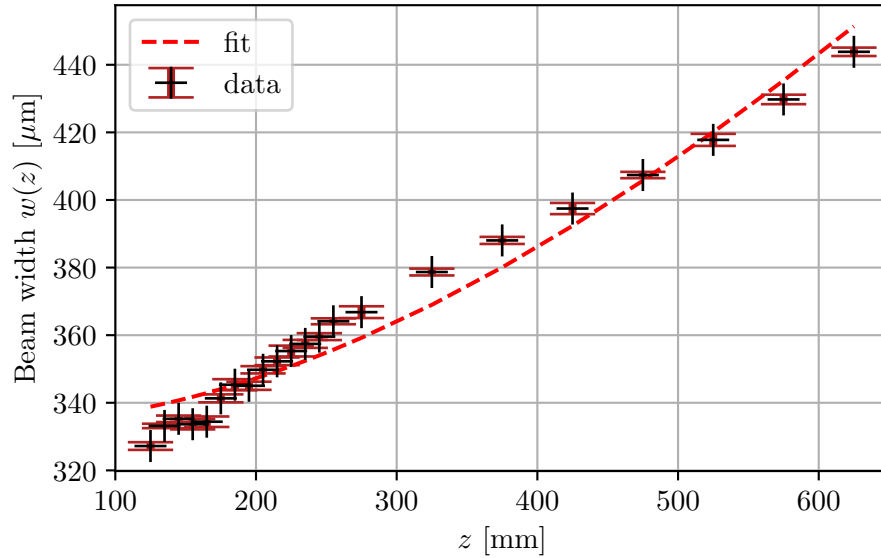


Figure 3: Tabulated data as in Table 1 and fitted beam profile.

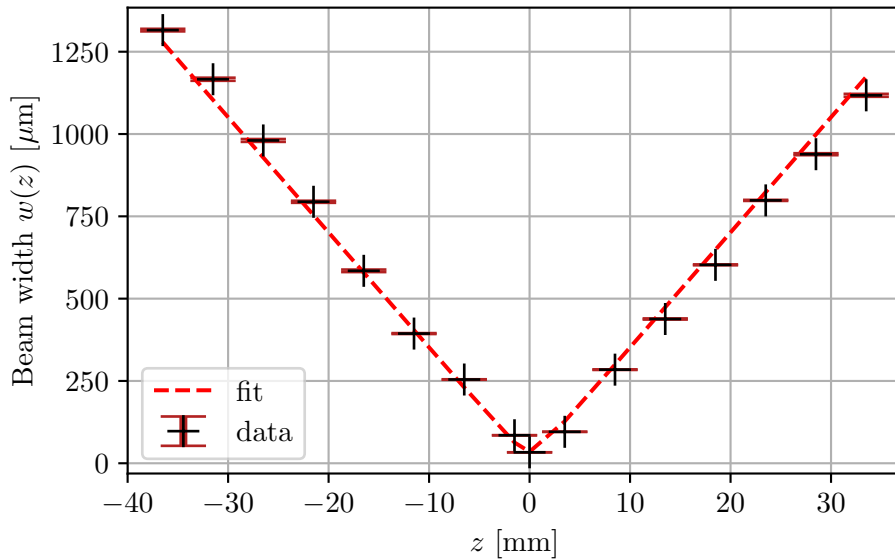


Figure 4: Tabulated data as in Table 2 and fitted beam profile.

2 ORBITAL ANGULAR MOMENTUM BEAM GENERATION

In this section we see an example of orbital angular momentum and comment on some of its properties.

Beams carrying orbital angular momentum (OAM) have a helical phase front and a field strength with a singularity along the axial center, which can be used for information transmission, imaging and particle manipulation.

A central idea is that of **optical vortex**, where the planes of constant phase of the electric and

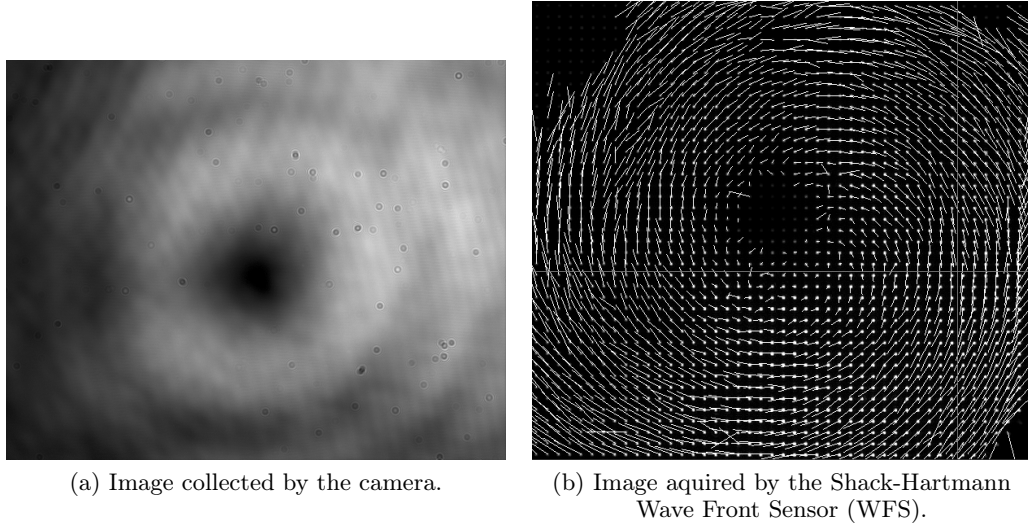


Figure 5: OAM beam generation.

magnetic vector fields form a corkscrew (or helicoid) running in the direction of propagation. The vortex is characterized by a number, called the **topological charge**, which indicates the number of twists the light does in one wavelength: the larger the number of twists, the faster the light is rotating around the axis.

The vortex waves are characterised by helical phase fronts: the amplitude of the vortex wave field is null along the axis center so that there is a “dark” core at the location of the phase singularity (Fig. 5, (a)).

A vortex beam can either be obtained as the direct output of a laser cavity, or can be generated by feeding a Gaussian beam into a converter, such as a cylindrical lens, a spiral phase plate, a phase hologram or a q-plate. In Fig. 5, (b) we can see the reconstructed wavefront captured by the Shack-Hartmann Wave Front Sensor (WFS), which provide accurate measurements of its shape and the intensity distribution of incident beams. In particular, the image obtained is a discrete vector field (as are the phase gradients) and the magnitudes of the vectors indicate the topological charges.

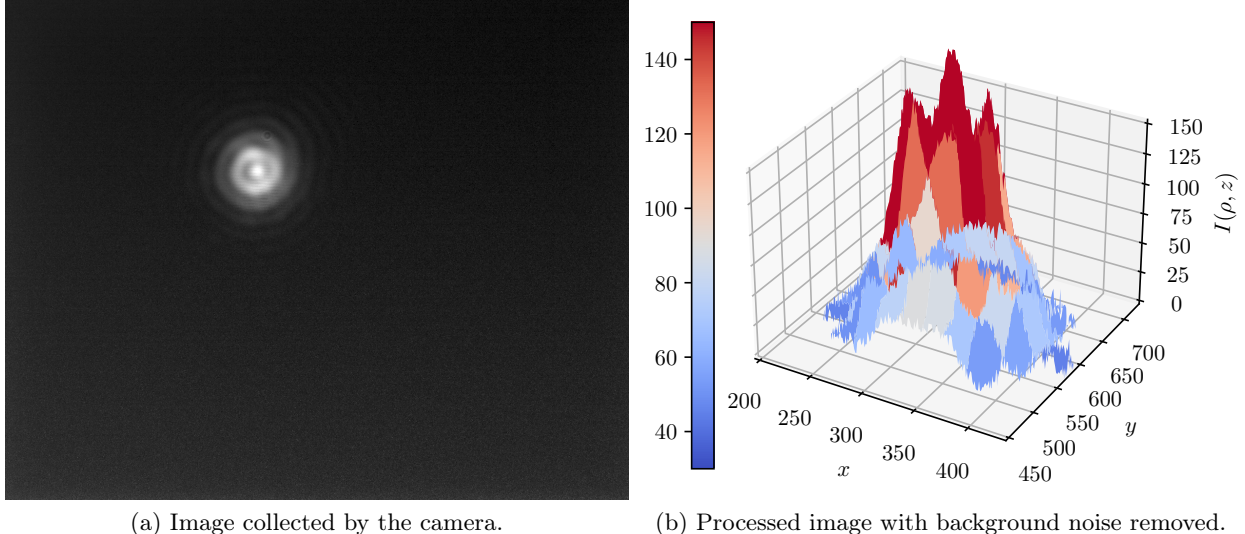
3 FRESNEL DIFFRACTION

The goal of this section is to estimate the diameter of the circular aperture a (interposed between source and detector) responsible for the interference phenomena observed.

3.1 THEORETICAL BACKGROUND AND EXPERIMENTAL SETUP

Compared to the previous case, the setup introduces:

- a **beam expander**, i.e. an optical device used to expand the cross-section (spot) of a collimated beam;
- a diaphragm with adjustable aperture (in place of the converging lens).

Figure 6: Example of the processing of raw images, $z = 140$ mm.

Diffraction occurs when a wave encounters an obstacle or opening. The diffracting object or aperture effectively becomes a secondary source of the propagating wave.

The phenomenon is described by the **Huygens–Fresnel principle** that treats each point in a propagating wavefront as a collection of individual spherical wavelets. The characteristic bending pattern is most pronounced when a wave from a coherent source (such as a laser) encounters a slit/aperture that is comparable in size to its wavelength.

In particular, a Gaussian beam incident on a slit of radius a satisfying the condition distance $w(z') \gg a$ - where z' is the distance of the iris from the source - is approximated, relative to the size of the element considered, by a plane wave. Through

$$N_F = \frac{a^2}{z \cdot \lambda}, \quad (6)$$

with N_F being the **Fresnel number** (i.e. the number of peaks in the intensity profile associated with an arbitrary section going through the centre of the image) and z the distance of the camera from the aperture, an estimate of a is given.

3.2 DATASET AND ANALYSIS

We consider 5 images collected as in Section 1.3: an example is reported in Fig. 6. The analysis follows closely what was seen in Section 1.4: F_N can be easily obtained from the images themselves. We collect an estimate for each image of a to reach

$$a = (0.77 \pm 0.08) \text{ mm.}$$

4 CONCLUSION

In this work we have estimated the parameters characterising a Gaussian beam and a converging lens. The analysis has produced results consistent with the expected theory. After having concentrated on an example of orbital angular momentum beam generation, we estimated the radius of a diffraction slit.

The discrepancies found reflect the influence of spurious contributions (e.g. background noise, diffracting phenomena, etc.) that were neglected in the theoretical treatment: the very same image processing process, based on legitimate simplifications and approximations, contributes inevitably to the deviations from theory. However, the analysis is considered to have produced acceptable results.

- [1] B. E. A. Saleh and M. C. Teich, *Fundamentals of photonics; 2nd ed.*, Wiley series in pure and applied optics (Wiley, New York, NY, 2007).